1	
2	
3	3-His Metal Coordination Site Promotes the Coupling of Oxygen Activation to Cysteine
4	Oxidation in Cysteine Dioxygenase
5	
6	
7	
8	
9	
10	
11 12 13	Dianna L. Forbes <sup>1</sup> , Kathleen M. Meneely <sup>2</sup> , Annemarie S. Chilton <sup>2</sup> , Audrey L. Lamb <sup>2</sup> , and Holly R. Ellis <sup>1</sup> *
14 15	<sup>1</sup> The Department of Chemistry and Biochemistry, Auburn University, Auburn, Alabama 36849
16 17 18	<sup>2</sup> Molecular Biosciences, University of Kansas, 1200 Sunnyside Avenue, Lawrence, KS 66045 USA.
19	
20	
21	Corresponding Author, *Email: ellishr@auburn.edu. Phone: (334) 844-6991.
22	
23	
24	
25	
26	

### Abstract

1

2

3

4

5

6

7

8

9

10

11

12

13

14

15

16

17

18

19

Cysteine dioxygenase (CDO), structurally resembles cupin enzymes that use a 3-His/1-Glu coordination scheme. However, the glutamate ligand is substituted with a cysteine (Cys93) residue, which forms a thioether bond with tyrosine (Tyr157) under physiological conditions. The reversion variant, C93E CDO, was generated to reestablish the more common 3-His/1-Glu metal ligands of the cupin superfamily. This variant provides a framework to test the structural and functional significance of Cys93 and the crosslink in CDO. Although dioxygen consumption is observed with C93E CDO, it was not coupled with L-cysteine oxidation. Substrate analogs (D-cysteine, cysteamine, 3-mercaptopropionate) were not viable substrates for the C93E CDO variant, although they showed variable coordination to the iron center. The structures of C93E, crosslinked and noncrosslinked wild-type CDO were solved by X-ray crystallography to 1.91 Å, 2.49 Å, and 2.30 Å, respectively. The C93E CDO variant had similar overall structural properties as crosslinked CDO, but the iron was coordinated by a 3-His/1-Glu geometry leaving only two coordination sites available for dioxygen and bidentate L-cysteine binding. The hydroxyl group of Tyr157 shifted in both non-crosslinked and C93E CDO, and this displacement prevents this residue from participation in substrate stabilization. Based on these results, divergence of the metal center of cysteine dioxygenase from the 3-His/1-Glu geometry seen with many cupin enzymes was essential for effective substrate binding. Substitution of Glu with Cys in CDO allows for a third coordination site on the iron for bidentate cysteine and monodentate oxygen binding.

## Introduction

Cysteine dioxygenase is an iron-dependent enzyme that catalyzes the conversion of L-cysteine to cysteine sulfinic acid (**Scheme 1**).<sup>1,2</sup> Unlike L-cysteine, cysteine sulfinic acid (CSA) is not itself a metabolically significant molecule. Instead, CSA serves as a major branch point in the catabolism of cysteine in mammals, and is further metabolized to pyruvate and sulfite or taurine.<sup>1,2</sup>

O C SH O C C SH CDO 
$$C$$
 Cysteine Sulfinic acid

Scheme 1. CDO reaction.

Cysteine dioxygenase belongs to the cupin superfamily, which is characterized by a double-stranded β-helix (DSBH) (**Figure 1A**).<sup>3–5</sup> The DSBH fold typically consists of six to eight beta sheets that fold in half creating a sandwich-like casing around the active site.<sup>6</sup> While some enzymes, including CDO, contain a coordinated iron, other cupin enzymes possess a nickel, zinc, manganese, cobalt, or copper metal center.<sup>1,7–12</sup> These different metal cofactors allow for the diverse enzyme activities observed within this family that include isomerase, decarboxylase, dioxygenase, cyclase, and epimerase reactions. Proposed reaction mechanisms of the metal-dependent cupins generally involve sequential binding of the substrate and dioxygen to the catalytic metal cation.

The enzymatic cupins were initially characterized by two conserved sequence motifs,  $GX_5HXHX_{3-6}EX_6G$  and  $GX_{5-7}PXGX_2HX_3N$ , containing the amino acid ligands that coordinate the metal (highlighted in bold). <sup>6,13</sup> Metals in enzymatic cupins are often coordinated by 3-His and 1-Glu located within the two conserved motifs (**Figure 1B**). <sup>14</sup> The 3-His/1-Glu ligand occupies

four coordination sites with solvent molecules occupying the remaining sites. A nitrogen of each histidine coordinates monodentate to the metal, while the glutamate coordinates the metal by the Oɛ-1 atom oxygen of the carboxyl group. In enzymatic cupins, the resting state of the metal center can exhibit different geometries, including octahedral, tetrahedral, trigonal bipyramidal, and square pyramidal geometries.<sup>4,5,9,15,16</sup> However, the substrate bound metal cation often exhibits octahedral geometry, allowing for a total of six coordination sites.

The active site of cysteine dioxygenase contains a modification to the common 3-His/1-Glu cupin motif. The glutamate residue is replaced by a noncoordinating cysteine (Cys93), leaving iron weakly coordinated by three histidine residues. Interestingly, the noncoordinating cysteine residue forms a thioether bond with a nearby tyrosine (Tyr157) residue (**Figure 1C**). Wild-type

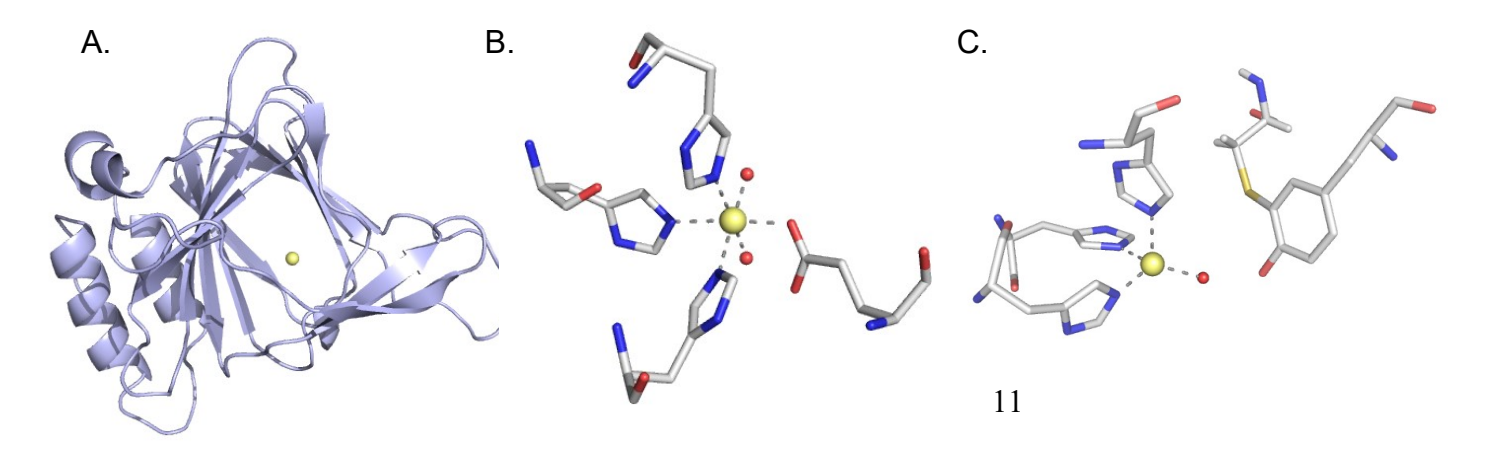


**Figure 1**. Overall structure and metal coordination motifs of cupin enzymes. **A.** CDO exhibits a β-barrel fold characteristic of the cupin superfamily (PDB: 6U4S). **B.** Acireductone dioxygenase has a characteristic 3 His/1 Glu coordination metal center (PDB: 2HJI). <sup>14</sup> **C.** The 3-His iron coordination motif of CDO is shown. A thioether crosslink between C93 and Y157 is positioned near the iron center (PDB: 6U4S). Ferric iron are shown as yellow spheres, and water molecules are red spheres.

1 rat CDO heterologously expressed in E. coli exists as an approximate equal mixture of non-

2 crosslinked and crosslinked isoforms. <sup>17,18</sup> These isoforms resolve on SDS-PAGE as two distinct

bands with the non-crosslinked isoform representing the upper molecular weight band. 19,20 While

the Cys-Tyr crosslink is not required for product formation, the crosslink enhances catalytic

5 efficiency.<sup>20,21</sup> There have been several proposed roles for the thioether crosslink since the initial

structural determination of CDO. Although not essential for catalysis, formation of the crosslink

may properly position the hydroxyl group of Tyr157 for optimal substrate binding. 5,20,22-25 It has

been suggested that formation of the crosslink leads to a pre-ordered state for substrate binding.<sup>21</sup>

Additional studies suggest that the thioether crosslink may also prevent competing side reactions

10 of Cys93.<sup>24,26</sup>

Alternative metal binding has been observed with proteins that comprise the cupin superfamily. Therefore, it is unclear how divergence of the metal center from a 3 His/1 Glu to a 3 His iron binding site affects the functional properties of the enzyme. Although studies have been performed to compare the 3-His coordination of CDO to the more conventional 2-His/1-Glu motif, there have been no direct studies to evaluate the catalytic benefit of the 3-His motif relative to the 3-His/1-Glu motif. Herein, the conserved Cys93 residue was replaced with glutamate to determine how the substitution alters the kinetic and structural properties of the enzyme compared to the wild-type enzyme. These studies were augmented with the first three-dimensional structure of non-crosslinked wild-type CDO to compare the position of Cys93 in the active site to the Glu substituted variant.

### **Materials and Methods**

### Materials

1

2

3 4-(2-Hydroxyethyl)piperazine-1-ethanesulfonic acid (HEPES), L-cysteine, D-cysteine, 4 cysteamine, 3-mercaptopropionic acid (3-MPA), L-ascorbate, ammonium sulfate, ampicillin, 5 streptomycin sulfate, lysozyme, and brilliant blue R were purchased from Sigma (St. Louis, MO). 6 Isopropyl-β-D-thiogalactoside (IPTG) was purchased from Gold Biotechnology (St. Louis, MO). 7 Glycerol and sodium chloride were purchased from Macron Fine Chemicals (Center Valley, PA). 8 Difco-brand Luria-Bertani (LB) media was purchased from Becton Dickinson and Company (Sparks, MD). Macro-Prep® High Q Support column media was purchased from Bio-Rad 9 10 Laboratories (Hercules, CA). 11 Construction and purification of C93E CDO The expression vector for rat C93E CDO was constructed through PCR amplification using 29 12 13 base oligonucleotide primers that replace the wild-type Cys codon with the Glu codon (GAA). The 14 PCR product containing the Cys to Glu substitution was confirmed by DNA sequence analysis 15 (Davis Sequencing, Davis, CA), and the C93E CDO vector was transformed into BL21 (DE3) 16 competent E. coli cells and stored as 20% glycerol stock at -80 °C. Expression and purification of wild-type and C93E CDO was carried out as previously described. 28 Expression of non-crosslinked 17 wild-type CDO was carried out in the presence of 1,10-phenanthroline as previously described.<sup>21</sup> 18 19 Ferrozine was used to determine the amount of iron present as previously described with slight modifications.<sup>29</sup> CDO samples (40 µM) were incubated at 95 °C for 5 minutes with ferrozine 20 21 (250 µM) and ascorbate (18 mM). After 5 mins, sodium acetate (1.5 M) was added and the samples 22 were measured at 562 nm. A standard curve (5-30 µM) was created using iron ICP standards and

1 the standards were treated the same as the CDO samples. The results were based on the average of

three separate experiments.

### Circular dichroism

Protein samples were buffer exchanged with 10 mM potassium phosphate, pH 7.5, using a 10 000 kDa MWCO Amicon Ultra Centrifugal Filters (Millipore) at 5000 RPM, 4°C. Far-UV circular dichroism spectra were recorded on a JASCO J-810 spectropolarimeter. Spectra of wild-type and C93E CDO (10 μM) were taken in 0.1 nm increments in continuous scanning mode from 300 to 185 nm in a 0.1 cm cuvette with a bandwidth of 1 nm and scanning speed of 20 nm/min. Each spectra is an average of six scans. Background subtraction and smoothing of the data were performed using the software provided. Final data were plotted using KaleidaGraph<sup>™</sup> software

# Steady-state kinetic analysis of wild-type and C93E CDO

(Synergy Software, Reading, PA).

Steady-state kinetic parameters were determined using a Clark-type oxygen electrode monitoring the rate of dioxygen utilization. Each assay contained a final concentration of 2  $\mu$ M enzyme and 1 mM ascorbate in 25 mM HEPES, pH 7.5, at 37 °C. The assays were initiated by the addition of L-cysteine substrate (50  $\mu$ M to 5 mM), and the initial velocities (nmol of oxygen consumed per second) were measured from the linear portion of the trace. The  $v_0$ /[Et] was corrected for the amount of iron present and plotted against the substrate concentration. Steady-state kinetic parameters were determined by fitting the averaged data from four individual experiments to the Michaelis-Menten equation using KaleidaGraph<sup>TM</sup> software (Synergy Software, Reading, PA). Substrate analogs D-cysteine, cysteamine, and 3-MPA were also tested for dioxygen consumption and product formation using the same protocol.

## Activity and product analysis of wild-type and C93E CDO

Cysteine sulfinic acid (CSA) or hypotaurine formation were quantified independently using mass spectrometry (MS) and correlated with the rate of dioxygen consumption. Assay conditions were similar to the dioxygen consumption assay, and reactions were initiated with the addition of 1 mM L-cysteine or cysteamine. After one minute the reaction was quenched with 1 μL formic acid (90% v/v). Acetonitrile was added to the quenched reaction in a 1:1 ratio (v/v). Mass analysis was performed on an Ultra Performance LC System (ACQUITY, Waters Corp., Milford, MA, USA) in-line with a quadrupole time-of-flight mass spectrometer (Q-Tof Premier, Waters) and electrospray ionization (ESI-MS) in negative mode. Cysteine sulfinic acid hypotaurine concentrations were determined against a CSA or hypotaurine standard curve which ranged from 50 - 200 μM (Figure 2).

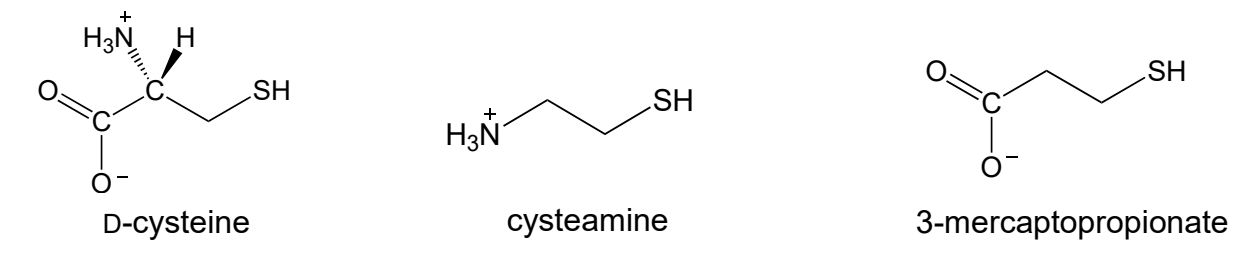


**Figure 2**. Structural analogs of L-cysteine: D-cysteine, cysteamine (2-aminoethanethiol), and 3-mercaptopropionic acid (3-MPA).

EPR spectroscopy

Electron paramagnetic resonance (EPR) studies were performed on a Bruker EMX spectrometer at X-band frequency (Bruker Biospin Corporation, Billerica, MA). Cooling to 9.8 K was performed using an Oxford Instruments ESR 900 flow cryostat and an ITC4 temperature controller. EPR analysis was performed with 100 μM CDO or C93E CDO as purified in 25 mM HEPES, 10% glycerol, pH 7.5, with 0.1 M NaCl. Samples containing a final concentration of 10

1 mM L-cysteine or substrate analogs (D-cysteine, cysteamine, and 3-MPA) were incubated with

2 100 μm enzyme on ice for 1 min and then flash frozen in EPR tubes with liquid nitrogen. All

spectra were recorded using the following settings: 9.39 GHz microwave frequency, 1.99 mW

microwave power, 2 x 10<sup>4</sup> or 4 x 10<sup>4</sup> receiver gain, 100 kHz modulation frequency, 6 G modulation

amplitude, with a time constant of 163.84 ms, and a sweep time of 167.77 s.

# Crystallization and diffraction data collection

Crystals were grown at 24°C using the hanging drop method. The reservoir solution for wild-type CDO contained 1 M lithium chloride, 22.5% (w/v) poly(ethylene glycol) (PEG) 10,000 in 0.1 M MES, pH 5.5, and the reservoir buffer for non-crosslinked wild-type CDO contained 1 M lithium chloride, 24% (w/v) poly(ethylene glycol) (PEG) 20,000 in 0.1 M MES at pH 6.5. Reservoir buffer of C93E CDO contained 1 M lithium chloride, 30% PEG 6,000 in 0.1 M sodium acetate. Each drop contained 1.5 μL of protein at 13 mg/ml for wild-type CDO or 11 mg/ml for non-crosslinked CDO in 50 mM Tris pH 8, 100 mM NaCl or 5 mg/ml C93E CDO in 25 mM HEPES pH 7.5, 100 mM NaCl 10% (v/v) glycerol mixed with an equal volume of reservoir solution. Drops containing wild-type and non-crosslinked wild-type CDO were microseeded immediately with 0.3 μL C93E CDO crystals in 1 M lithium chloride, 25% (w/v) PEG 6,000, 0.1 M MES, pH 5.5. Crystals were formed after one day and grew to full size within four days. For data collection, crystals were serially washed in 1 M lithium chloride, 30% PEG 6,000 in 0.1 M sodium acetate supplemented with 20% (w/v) sucrose as a cryoprotectant and flash cooled to -160°C.

Wild-type CDO diffraction data (0.15° oscillation images for a total of 83°) were collected remotely at the Stanford Synchrotron Radiation Laboratory (SSRL, Stanford, CA) on beamline

- 1 12-2 at a wavelength of 0.9795 Å at 100 K using Blu-Ice. 30 The exposure time per frame was 0.5
- s with 79.5% attenuation and a crystal to detector distance of 344.6 mm. The data were indexed
- and scaled with XDS to 2.49 Å.<sup>31</sup> The crystals were assigned to the space group P4<sub>1</sub>2<sub>1</sub>2 with unit
- 4 cell dimensions a = b = 57.5 Å and c = 122.3 Å (**Table 1**).
- Non-crosslinked wild-type CDO diffraction data (0.15° oscillation images for a total of
- 6 114°) were collected at SSRL beamline 12-2 at a wavelength of 0.9795 Å at 100 K using Blu-Ice.
- 7 The exposure time per frame was 0.4 s with 73.5% attenuation and a crystal to detector distance
- 8 of 359.1 mm. The data was indexed and scaled with XDS to 2.30 Å. The crystals were assigned to
- 9 the space group  $P4_12_12$  with unit cell dimensions a = b = 57.6 Å and c = 122.5 Å (**Table 1**).
- 10 C93E CDO diffraction data (0.4° oscillation images for a total of 360°) were collected
- remotely on SSRL beamline 7-1 at a wavelength of 1.1271 Å at 100 K using Blu-Ice. The exposure
- time per frame was 5.71 s with 2.2% attenuation and a crystal to detector distance of 243.6 mm.
- 13 The data was indexed and scaled with XDS to 1.91 Å. The crystals were assigned to the space
- group  $P4_12_12$  with unit cell dimensions a = b = 57.7 Å and c = 122.2 Å (**Table 1**).
- Molecular replacement calculations were performed using Phaser in the PHENIX program
- suite, using PDB: 2B5H as the search model with iron and waters removed yielding a clear solution
- with each structure. <sup>4,32</sup> Log likelihood gains ranged from 2282 9483 with TFZ scores of 48 94.
- Model building and refinement were performed using Coot and Phenix Refine. 32,33 Root mean
- square deviation (RMSD) calculations were obtained with lsqkab from ccp4.<sup>33</sup> The final structure
- 20 for wild-type CDO includes residues 6-190 with no missing intervening residues, 1 Fe, and 5 water
- 21 molecules with 97.8% of the residues in favored Ramachandran angles and the remaining 0.2% in
- 22 allowed regions. The structure of non-crosslinked wild-type CDO includes residues 6-190 with
- 23 99.5% of the residues in favored regions of the Ramachandran plot and the remaining 0.5% in

- 1 allowed regions, 1 Fe and 19 water molecules. The structure of C93E CDO consists of residues 6-
- 2 189, 1 Fe, 1 acetate ion, and 84 water molecule with 99.4% of the residues with favorable
- 3 Ramachandran angles and 0.6% in the allowed regions. None of the structures contain any residues
- 4 with unfavorable Ramachandran angles; however, all three structures contain a single residue
- 5 change E46D from the published structure (PDB: 4FX0). E46D is an external, solvent exposed
- 6 residue, and this is likely an artifact of the cloning source.

Table 1: Data collection and refinement statistics for wild-type and C93E CDO

	crosslinked CDO	non-crosslinked CDO	C93E CDO
	PDB: 6U4S	PDB: 6U4V	PDB: 6U4L
Data collection <sup>a</sup>			
Beamline	12-2	12-2	7-1
Wavelength (Å)	0.9795	0.9795	1.1271
Space group	P4 <sub>1</sub> 2 <sub>1</sub> 2	P4 <sub>1</sub> 2 <sub>1</sub> 2	$P4_{1}2_{1}2$
Cell dimensions: $a, b, c$ (Å), $\beta$ (°)	57.5, 57.5, 122.3	57.6, 57.6, 122.5	57.7, 57.7, 122.2
Resolution (Å)	38.6 - 2.49	38.6 - 2.30	38.7 - 1.91
	(2.59 - 2.49)	(2.38 - 2.30)	(1.96 - 1.91)
$R_{\mathrm{merge}}^{}}$	0.082 (0.452)	0.116 (0.459)	0.085 (0.417)
Total observations	43530 (4665)	75791 (6100)	451694 (18259)
Total unique observations	7638 (809)	9683 (857)	16741 (1068)
Mean $((I / sd(I))$	13.5 (3.1)	13.0 (4.2)	33.4 (7.4)
Completeness (%)	99.2 (96.7)	99.4 (94.2)	99.9 (98.2)
Redundancy	5.7 (5.8)	7.8 (7.1)	27.0 (17.1)
Refinement			
Resolution (Å)	38.6 - 2.49	38.6 - 2.30	38.7 - 1.91
Resolution (A)	(2.68 - 2.49)	(2.42 - 2.30)	(1.97 - 1.91)
$R_{\mathrm{cryst}}^{\mathrm{c}}$	0.178 (0.230)	0.175 (0.194)	0.174 (0.176)
$R_{ m free}$	0.261 (0.327)	0.233 (0.315)	0.215 (0.239)
Total unique observations	7599 (1307)	9435 (1098)	16517 (1154)
No. of non-hydrogen atoms			
Protein	1502	1502	1481
Iron	1	1	1
Ligand	0	0	4
Water	5	19	84
rms deviation bonds (Å)	0.015	0.013	0.01
rms deviation angles (°)	1.28	1.14	1.04
Overall mean B-factor (Å <sup>2</sup> )	36.9	20.5	18.4
Ramachandran plot analysis <sup>d</sup>			
Favored region	97.81	99.45	99.44
Allowed region	2.19	0.55	0.56
Outlier region	0.00	0.00	0.00

<sup>&</sup>lt;sup>a</sup>data indexed and scaled with XDS

 $<sup>{}^{</sup>b}R_{merge} = \Sigma_{h}|I_{h} - \langle I \rangle|/\Sigma_{h}I_{h}$ , where  $I_{h}$  is the intensity of reflection h, and  $\langle I \rangle$  is the mean intensity of all symmetry-related

 $<sup>{}^{</sup>c}R_{cryst} = \Sigma ||F_o| - |F_c||/\Sigma |F_o|$ ,  $F_o$  and  $F_c$  are observed and calculated structure factor amplitudes. Five percent of the relections were reserved for the calculation of  $R_{free}$ .

<sup>&</sup>lt;sup>d</sup>Calculated with Molprobity.<sup>54</sup>

### Results

# Characterization of wild-type and C93E CDO

Purified wild-type and C93E CDO enzymes were evaluated for crosslink formation by SDS-PAGE (**Supplemental Figure S1**). Wild-type CDO existed as a heterogeneous mixture of both non-crosslinked and crosslinked isoforms as seen previously; whereas, non-crosslinked CDO migrated as a single band similar to the higher molecular weight band seen in wild-type CDO. 19,20 Because C93E CDO lacks the cysteine involved in formation of the thioether crosslink, the variant enzyme existed solely as the non-crosslinked isoform. Far-UV circular dichroism (CD) spectra of wild-type and C93E CDO were recorded to determine if the variant had altered overall gross secondary structure. The C93E CDO variant showed a comparable CD trace to crosslinked wild-type CDO (**Supplemental Figure S2**). The iron content of C93E CDO following dialysis was 50 ± 2% similar to non-crosslinked CDO at ~ 50% iron. 20

## Steady-state kinetic properties of wild-type and C93E CDO

Kinetic properties of wild-type and C93E CDO were determined by measuring the rate of dioxygen consumption using a Clark-type oxygen electrode (**Supplemental Figure S3**). The  $k_{\text{cat}}/K_{\text{m}}$  value for C93E CDO with L-cysteine as substrate was  $450 \pm 80 \text{ M}^{-1} \text{ s}^{-1}$  resulting in a ~78-fold decrease in oxygen consumption compared to wild-type (35,000  $\pm$  6,000 M<sup>-1</sup> s<sup>-1</sup>) (**Table 2**). Wild-type CDO is specific for L-cysteine, and has a reduced specificity constant for substrate analogs. Wild-type CDO showed  $k_{\text{cat}}/K_{\text{m}}$  values for D-cysteine of  $1200 \pm 600 \text{ M}^{-1} \text{ s}^{-1}$  and cysteamine of  $1000 \pm 300 \text{ M}^{-1} \text{ s}^{-1}$ , and there was no oxygen consumed with 3-mercaptopropionic acid (**Table 3**). The kinetic parameters for C93E CDO were also determined with L-cysteine analogs to determine if alternative substrates could be utilized by the variant. For C93E CDO, the  $k_{\text{cat}}/K_{\text{m}}$  values were comparable, within error, with L-cysteine (450  $\pm$  80), D-cysteine (300  $\pm$  200

- 1  $M^{-1}$  s<sup>-1</sup>), or cysteamine (800 ± 300  $M^{-1}$  s<sup>-1</sup>) as substrates (**Table 2**), and the variant showed no
- 2 dioxygen consumption with 3-mercaptoproionic acid.

**Table 2:** Steady-state kinetic parameters measuring oxygen consumption with L-cysteine.<sup>a</sup>

L-cysteine. <sup>a</sup>					
	$k_{\rm cat}$ (s <sup>-1</sup> )	$K_{\rm m}$	$k_{\rm cat}/K_{ m m} \ ({ m M}^{-1}{ m s}^{-1})$	4	
	(S )	(μΜ)	(NI S )	5	
wild-type CDOb	$2.1\pm0.1$	$60 \pm 10$	$35,000 \pm 6,000$	J	
				6	
C93E CDO	$0.14 \pm 0.02$	$320 \pm 100$	$450 \pm 80$		
				7	
<sup>a</sup> Kinetic parameters adjusted for iron content.					
<sup>b</sup> Previously reporte	$ed.^{2I}$			8	
<sup>b</sup> Previously reported. <sup>21</sup>					

Table 3: Steady-state kinetic parameters measuring oxygen consumption with L-cysteine analogs.<sup>a</sup>

	wild-type CDO		C93E CDO			
	$k_{\rm cat}$ (s <sup>-1</sup> )	K <sub>m</sub> (mM)	$k_{\rm cat}/K_{\rm m} \ ({ m M}^{-1}{ m s}^{-1})$	$k_{\rm cat}$ (s <sup>-1</sup> )	K <sub>m</sub> (mM)	$k_{\text{cat}}/K_{\text{m}}$ $(M^{-1}s^{-1})$
D-cysteine	$0.25\pm0.02$	$0.2 \pm 0.09$	$1200 \pm 600$	$0.20 \pm 0.03$	$0.7\pm0.4$	$300\pm200$
cysteamine	$1.1\pm0.1$	$1.1\pm0.3$	$1000\pm300$	$1.2 \pm 0.2$	$1.6\pm0.6$	$800\pm300$
3-mercaptopropionate	_b	_	_	_	_	_

<sup>&</sup>lt;sup>a</sup> Kinetic parameters adjusted for iron content.

9

10

11

12

13

14

15

16

# Analysis of cysteine sulfinic acid and hypotaurine product

Mass spectrometric analyses were performed to correlate product formation with dioxygen utilization utilizing L-cysteine and cysteamine. Wild-type CDO formed CSA from L-cysteine at a rate of  $4000 \pm 200$  nmol min<sup>-1</sup> mg<sup>-1</sup>, which correlated with  $4300 \pm 200$  nmol min<sup>-1</sup> mg<sup>-1</sup> of  $O_2$  consumed (**Table 4**). Despite measured oxygen utilization, C93E CDO did not form CSA at detectable levels with L-cysteine as substrate. Because cysteamine lacks a carboxyl group, it may generate the product hypotaurine if cysteamine is able to bind monodentate to the metal center.

<sup>&</sup>lt;sup>b</sup> There was no measurable activity under the described experimental conditions.

- When cysteamine was used as a substrate, both wild-type and C93E CDO exhibited comparable rates for dioxygen utilization. However, neither wild-type or C93E CDO were able to form
- 3 hypotaurine.

**Table 4:** Dioxygen utilization and cysteine sulfinic acid production of wild-type and C93E CDO with L-cysteine and cysteamine substrates.

	L-cysteine		cysteamine		
	wild-type CDO	C93E CDO	wild-type CDO	C93E CDO	
Dioxygen utilization (nmol/min/mg)	$4300\pm200$	$270\pm20$	$950\pm20$	$1280\pm10$	
Cysteine sulfinic acid production (nmol/min/mg)	$4000\pm200$				

# 

# EPR analyses of wild-type and C93E CDO

EPR analyses were performed to evaluate the coordination environment of the iron in the as purified and substrate bound state of C93E CDO. Previous EPR studies showed wild-type CDO as purified under our purification conditions to have a high spin iron (III) oxidation state with a  $g = 4.3 \text{ signal.}^{29,35,37}$  However, the relative signal intensity has been shown to increase in the crosslinked isoform or with L-cysteine substrate bound. In addition, there is a shift to more rhombic iron(III) features with the resolution of three principal g-values with L-cysteine bound ( $g_{x,y,z}=4.47$ , 4.36, and 4.27). Wild-type and C93E CDO existed in the high spin rhombic iron (III) oxidation state with an EPR signal of g = 4.46 for wild-type and g = 4.43 for C93E CDO (**Figure 3A**). The g-values observed for wild-type CDO in these studies in the absence of L-cysteine differed from those previously reported. g-1,24,29,35,38

C93E CDO was incubated in the presence of L-cysteine, cysteamine, or 3-MPA to evaluate the effects of substrate on the iron coordination environment. Compared to resting state C93E

CDO, addition of substrates L-cysteine or 3-MPA resulted in an increase in the overall relative signal intensity, whereas there was no observable increase in the presence of cysteamine (**Figure 3B**). The *g*-values for cysteamine and L-cysteine with C93E CDO were comparable to the *g*-value obtained with C93E alone. There was a shift in the *g*-value for C93E CDO with 3-MPA to 4.38 compared to C93E CDO alone (g = 4.43). The shift in the *g*-value can be attributed to a change in the coordination environment of the iron center upon substrate binding.<sup>24</sup>

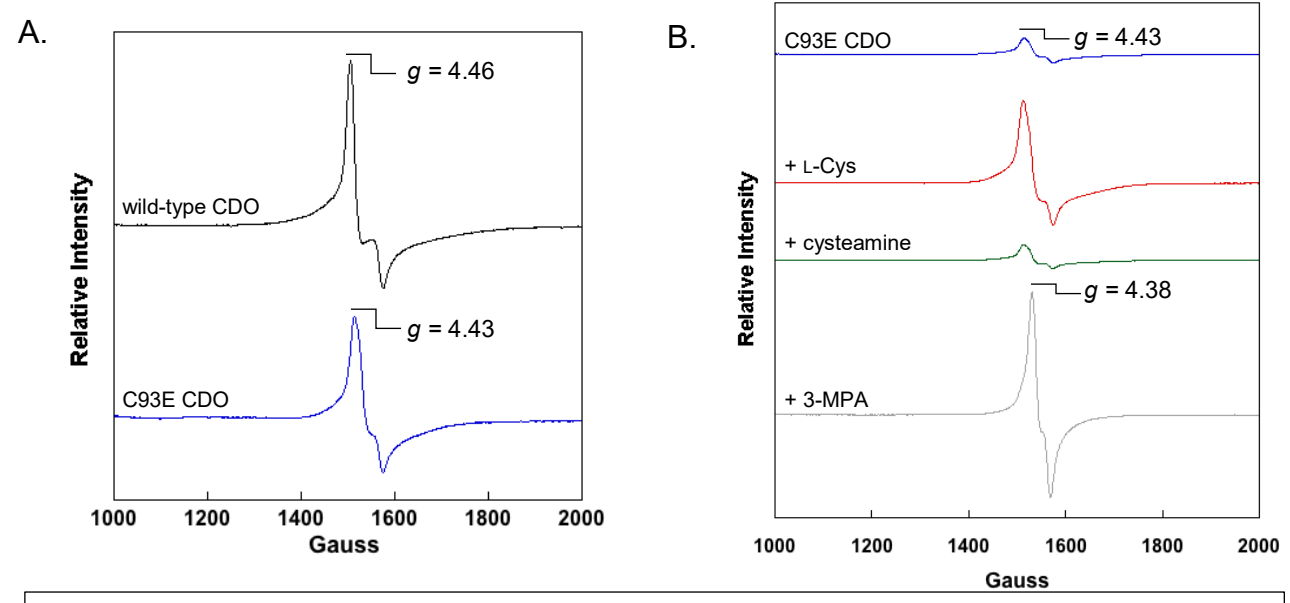


**Figure 3.** EPR spectra of wild-type and C93E CDO **A.** EPR spectra of wild-type (black trace) and C93E (blue trace) CDO. **B.** EPR spectra of C93E CDO (blue) with L-cysteine (red), cysteamine (green), and 3-MPA (gray). Spectra were taken with 100 μM protein in 25 mM HEPES buffer, pH 7.5, 10% glycerol, 100 mM sodium chloride.

# Three-dimensional structures of CDO

Crystal structures of crosslinked and non-crosslinked wild-type CDO were solved by molecular replacement and refined to 2.49 Å and 2.30 Å resolution, respectively. The C93E CDO variant was solved to 1.91 Å resolution. As anticipated, the structures show a high degree of similarity to the previously solved wild-type CDO structure (2B5H). The root mean square

deviation (rmsd) for both wild-type CDO isoforms were similar to the previously determined wildtype CDO structure (PDB 2B5H) (Table 1). Similar rmsd values were also observed for the crosslinked and non-crosslinked wild-type CDO structures, and crosslinked wild-type CDO to

4 C93E CDO (Table 1). The primary deviations were found in the active sites.

In both the crosslinked and non-crosslinked structures, the iron is coordinated by the three histidine residues and a water molecule in a tetrahedral coordination environment (**Figure 4A and C**). The iron in C93E CDO is also coordinated by the Nε-nitrogen on the imidazole ring of the same three histidine residues that coordinate the iron in wild-type CDO (**Figure 4B**). However, the Oε-1 atom of Glu93 now forms a ligand to the iron center, and is occupying the site that has been proposed to coordinate dioxygen in the wild-type enzyme (**Figure 4B**). <sup>22,36,39,40</sup> The other two coordination sites in the C93E CDO structure are occupied by a water and an acetate ion derived from the crystallization solution.

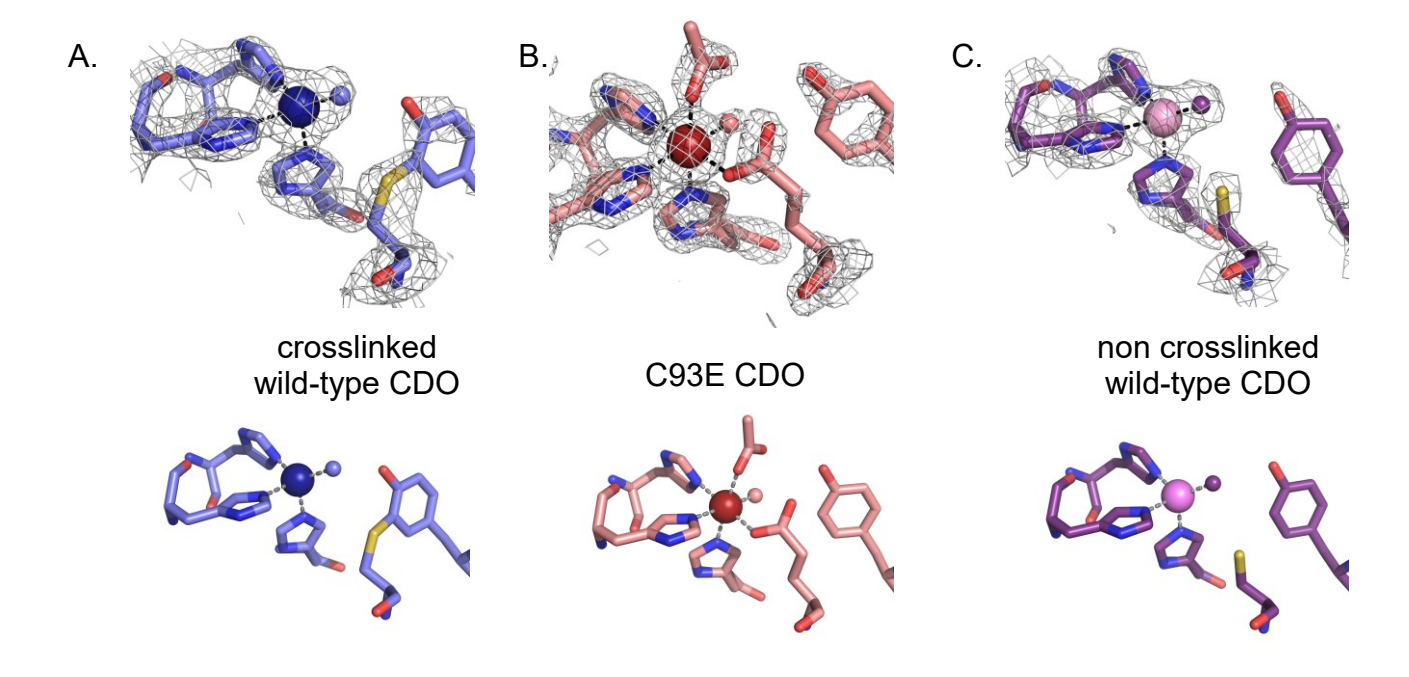


**Figure 4.** Active site structures of CDO. **A.** The iron center of crosslinked wild-type CDO is coordinated by 3 His residues, and the thioether crosslink is formed between Cys93 and Tyr157 (blue, PDB: 6U4S). **B.** The iron center in the C93E CDO structure is coordinated by a 3His/1 Glu motif. The oxygen atom of acetate derived from the crystallization solution is also coordinating the metal center (salmon, PDB: 6U4L). **C.** The iron center of non-crosslinked CDO is coordinated by 3 His residues, but the thioether crosslink between Cys93 and Tyr157 has not formed (purple, PDB: 6U4V). The electron density maps are simulated annealing composite omit maps contoured at 2.0 σ.

An overlay of crosslinked and non-crosslinked wild-type CDO active sites shows little deviation in the His ligands coordinating the active site metal center (**Figure 5A**). The Tyr157 that forms the thioether adduct in crosslinked CDO has shifted 1.4 Å away from Cys93 in the non-crosslinked structure. C93E CDO exists as the homogeneous non-crosslinked isoform due to the substitution of Cys93 with Glu. This allows for coordination of Glu93 to the iron center (2.1 Å). Tyr157 in the C93E CDO structure is similarly shifted 1.4 Å away from Glu93 due to the absence of a thioether crosslink, akin to the distance between Tyr157 and Cys93 in the non-crosslinked wild-type CDO structure. In the C93E CDO structure the bound water is displaced relative to the coordinating water in both the crosslinked and non-crosslinked wild-type CDO structures. In the C93E CDO structure there is also a slight shift in His88 away from the active site (0.6 Å) that shifts the iron in the active site resulting in a shift in His86 (0.4 Å). All of the other distances are within error to both the crosslinked and non-crosslinked structures.

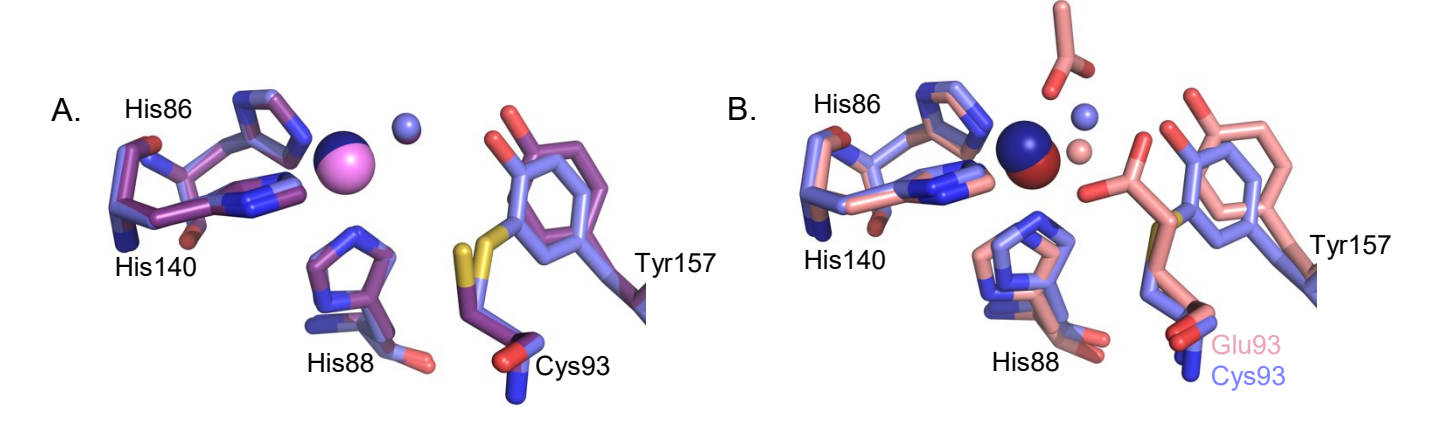


**Figure 5.** Overlay of the active sites. **A.** The non-crosslinked CDO ligands are shown in purple and the crosslinked CDO ligands are shown in blue. Tyr157 in non-crosslinked CDO has shifted 1.4 Å away from Cys93 compared to Tyr157 in crosslinked CDO. **B.** The C93E CDO ligands are shown in salmon and the crosslinked wild-type CDO ligands are shown in blue. Absence of the thioether crosslink shifts the hydroxyl group of Tyr157 1.4 Å away Glu93 compared to the Tyr157 in wild-type CDO.

#### **Discussion**

In 3-His/1-Glu cupin dioxygenases, single-site substrate coordination to the iron is not uncommon. Initial studies of cupin proteins identified two conserved motifs that were thought to be a defining feature among this superfamily.<sup>3,41</sup> Due to the extensive number of enzymes that belong to the cupin superfamily, it is difficult to determine the prevalence of this 3-His/1-Glu motif. As additional cupin proteins were identified, the idea of a defined conserved motif that defines the cupin family began to shift. Quercetin dioxygenase, an enzyme that catalyzes the first step in the degradation of quercetin, adopts the 3-His/1-Glu cupin motif. Both quercetin and dioxygen bind monodentate to the metal cation in a sequential ordered mechanism. It is important that quercetin only occupies one coordination site because bidentate binding of quercetin would occupy all metal sites leaving no room for dioxygen binding. In addition, monodentate binding of the bulky substrate allows it to remain flexible so unique distortion can occur, which is essential for oxygen incorporation and product formation. This monodentate binding of both substrates is a common mechanism for cupins with a 3-His/1-Glu metal binding site. While there are clearly enzymes that utilize a 3-His/1-Glu motif for metal coordination, other coordination geometries have also been identified within this family (3-His, 2-His/1-Glu, 2-His/1-Glu/1-Gln, and and 4-Cys).42-45

CDO contains a 3-His iron coordination center that diverges from the 3-His/1-Glu metal coordination site originally proposed for cupin enzymes. Like QDO, CDO follows an ordered sequential mechanism in which CDO binds L-cysteine first followed by dioxygen. The L-cysteine substrate binds bidentate to the Fe(II) center by the amino and thiol groups, and the carboxyl group is stabilized by a nearby arginine residue and the hydroxyl of the tyrosine involved in the thioether crosslink.<sup>40</sup> After L-cysteine coordinates, dioxygen binds monodentate occupying the remaining

coordination site.<sup>24,39</sup> For product formation in CDO, bidentate substrate coordination has been suggested to lower the reduction potential of Fe(II) so dioxygen can bind to the metal cation and form the Fe(III) peroxo intermediate.<sup>38,39</sup> Although it is known that both atoms of dioxygen are incorporated in the final cysteine sulfinic acid product, it is still unclear whether the oxygen proximal or distal to the iron reacts with the sulfur first.<sup>46</sup>

The Glu that coordinates the metal in some cupin enzymes is replaced by a Cys (Cys93) in CDO that forms a thioether crosslink with Tyr157. The sulfur of the cysteine residue at position 93 is too distant to coordinate the iron center. There are several proposed functional roles for the Cys-Tyr crosslink. The thioether adduct has been proposed to contribute to the stabilization of the coordinated substrates. Stabilization of substrate may occur through a pre-ordering of the active site to promote catalysis. Crosslink formation has also been proposed to protect Cys93 from potentially detrimental side reactions. Cysteamine dioxygenase (ADO) is a eukaryotic thiol dioxygenase that shares ~16% amino acid sequence identity with CDO. ADO was recently shown to form a thioether crosslink similar to CDO, but the role of the crosslink in catalysis has not been fully evaluated. There are two distinct bacterial cupin 3-His iron thiol dioxygenases that differ in their substrate specificities. Although the bacterial thiol dioxygenases contain an active-site Tyr, they are unable to form the cross-link because a Gly residue is in a comparable position as the thioether Cys in mammalian CDO. Society of the cysterior of the cysterior and comparable position as the thioether Cys in mammalian CDO.

As hypothesized, the substitution of Cys93 to a glutamate residue yielded the 3-His/1-Glu coordination environment exhibited by several cupin enzymes (**Figure 4B**).<sup>6</sup> In the three-dimensional structure, the carboxylate oxygen of Glu93 is coordinating the iron at the proposed dioxygen binding site. The lack of the thioether crosslink shifted Tyr157 1.4 Å away from Cys93. Cys93 in the non-crosslinked CDO structure was in a similar position as Glu93 in the C93E CDO

variant, and Cys93 remained unable to coordinate the metal due to the shorter side chain.<sup>23</sup> A structure of the Y157F CDO variant unable to form the crosslink, showed Cys93 in a similar conformation as both the Cys in non crosslinked CDO and Glu in C93E CDO. The Tyr157 in C93S CDO variant shifted 1.0 Å away from the iron. 23 There was a 1.0 Å shift in the Fl<sub>2</sub>-Tyr157 and a rotation of the aromatic ring in a non-crosslinked CDO structure containing fluorinated Tyr157.<sup>50</sup> It was noted that the rotation was likely due to the fluorinated Tyr. Substitution of the Gly bacterial MDO with Cys resulted in crosslink formation, but there was no activity observed.<sup>51</sup> In the noncrosslinked structure of the G95C MDO variant the Cys had shifted the active site Tyr. 51 Similarly, the shift of Tyr157 in the non-crosslinked structure away from Cys93 and the metal in the noncrosslinked structure of CDO would be unable to assist in stabilizing substrates. It should be noted that the hydroxyl of Tyr157 hydrogen bonds to the water liganded to the iron in the the wild-type CDO structure, but not the non-crosslinked or C93E CDO structures reported here. Previously, in variants unable to form the thioether crosslink, a chloride ion was hypothesized to replace the water molecule coordinated to the iron for crystals grown in the presence of 15 mM chloride. 40 Chloride was proposed to act as a potential inhibitor under physiological conditions. In the structures reported here, there is insufficient evidence to model the water molecule coordinating the iron in the crosslinked CDO structure as a chloride ion, despite the structures being determined from crystal grown in 1 M LiCl.

Wild-type CDO in the absence of substrate exhibited a similar g-value (g = 4.46) previously observed for crosslinked CDO or L-cysteine bound CDO.<sup>24,37</sup> Given that the EPR spectra was obtained in the absence of L-cysteine, the shift in g-value of wild-type CDO is likely attributed to the crosslinked species. EPR spectra of resting wild-type and C93E CDO showed comparable Fe(III) signals with different g-values (**Figure 3A**) The difference in g-values in the absence of L-

cysteine could be attributed to altered coordination of the iron center (3-His versus 3-His/1Glu).<sup>36</sup> In the presence of L-cysteine the relative signal intensity C93E CDO increased compared to the resting state, but there was no apparent shift in g-values (Figure 3B). This change in signal intensity was previously observed with substrate binding and/or formation of the thioether crosslink. 21,24,37 Given that the C93E CDO variant is unable to form the crosslink, the increased EPR signal observed for C93E CDO suggests L-cysteine is coordinating to the metal center (**Figure 6A**). The  $k_{cat}/K_m$  value for dioxygen utilization by C93E CDO was decreased ~78-fold compared to the wild-type enzyme with L-cysteine as substrate (Table 2), but the reduction of dioxygen was not coupled to oxidation of the L-cysteine thiol (Table 4). Therefore, the uncoupled dioxygen utilization observed in kinetic assays of C93E CDO suggests that dioxygen is also coordinating the metal center (Figure 6 B). This unproductive catalysis would produce reduced dioxygen uncoupled to L-cysteine substrate oxidation.<sup>39</sup> Alternatively, the utilization of dioxygen uncoupled to product formation could be due to an to an outer sphere oxidation in the C93E CDO enzyme. The Cys93-Tyr157 thioether crosslink is essential for efficient coupling in wild-type CDO due to the positoning of Tyr157 in the active site that contributes to substrate recognition and enzyme-substrate stabilization.<sup>24</sup> The absence of the crosslink could lead to a general instability in the active site resulting in the oxidation of active site amino acids.

Analogs of L-cysteine were evaluated to determine if the 3-His/1-Glu iron coordination altered the substrate specificity. Substrate analogs D-cysteine and cysteamine displayed similar catalytic efficiencies for dioxygen consumption with C93E CDO, whereas 3-MPA had no measurable activity (**Table 3**). The activity did not correlate with product formation with cysteamine for C93E CDO, similar to results obtained with the L-cysteine substrate (**Table 4**). There are conflicting reports on the ability of wild-type CDO to utilize cysteamine. Several groups

have been unable to detect product formation with cysteamine as substrate. <sup>35,36,52</sup> However, alternative studies have identified cysteamine product formation with a coupling efficiency ~100-fold lower than with L-cysteine. <sup>53</sup> When C93E CDO was incubated with cysteamine, the EPR *g*-value and signal intensity were comparable to the CDO variant in the absence of substrate, suggesting that cysteamine does not bind to the iron center. Cysteamine may bind with weak monodentate coordination of the sulfur or α-amino group to the metal center if substrate binding to the metal center is needed for dioxygen reduction (**Figure 6 C**). C93E CDO incubated in the presence of 3-MPA showed a shift in the *g*-value to 4.38 with an increase in the relative EPR signal intensity compared to C93E CDO with L-cysteine bound, supporting a more stable coordination of the substrate to the metal center. Bidentate binding of 3-MPA by the carboxylate group and thiol would prevent oxidation of the substrate thiol and dioxygen utilization observed with L-cysteine and cysteamine, and would also lead to the observed increase in the EPR signal intensity (**Figure 6D**).

These data lead to a connundrum. In the C93E CDO variant, where the glutamate replaces the putative dioxygen binding site, stable bidentate coordination of L-cysteine would prevent the binding of dioxygen, and activation of dioxygen by the ferrous iron.<sup>24</sup> Therefore, the reduced kinetic parameters of the C93E CDO variant may indicate that the glutamate ligand must be broken at some point in the catalytic cycle, which is initiated by bidentate binding of the L-cysteine substrate followed by monodentate binding of dioxygen. While dioxygen is reduced, no product formation is detected, which may suggest the glutamate, even when not liganding the iron, sterically hinders chemistry. An alternative option is that the C93E CDO variant may be binding the L-cysteine substrate in a monodentate fashion allowing dioxgen to coordinate the reduced metal center at a site different than previously proposed, which is now occupied by the glutamate ligand

(**Figure 6B**). This allows for reduction of dioxygen that is uncoupled from L-cysteine oxidation. However, it is not clear whether the α-amino group or thiol L-cysteine is coordinating the metal. **Conclusions:** The evolutionary divergence of the 3-His/1-Glu to a 3-His coordination environment in cysteine dioxygenase allows for multi-site occupancy of L-cysteine. Without the bidentate

coordination, the L-cysteine substrate may remain too flexible for proper cysteine oxidation to occur. The Glu to Cys variation at residue 93 provides a third free coordination site on the ferric iron and opens the active site sterically to allow for simultaneous binding of cyteine in a bidentate

## A. bidentate binding of L-cysteine

His<sub>88</sub> 
$$His_{140}$$
  $His_{86}$   $His_{86}$ 

## B. monodentate binding of L-cysteine

fashion and dioxygen in a monodentate fashion.

His<sub>88</sub> His<sub>140</sub>
His<sub>88</sub> His<sub>140</sub>
His<sub>86</sub>
Fe<sup>+3</sup>
SH
O
O
O
COO

coordination by the L-cysteine thiol

coordination by the  $\alpha$ -amino group

# C. monodentate binding of cysteamine

$$\begin{array}{c|c} \text{His}_{140} \\ \text{His}_{88} \\ \text{IIII}_{\text{IIII}} \\ \text{Fe}^{+3} \\ \text{Glu}_{93} \\ \text{O} \\ \text{O} \\ \text{O} \\ \text{O} \\ \text{O} \\ \end{array}$$

# D. monodentate binding of 3-MPA

His<sub>88</sub> His<sub>140</sub>
His<sub>88</sub> His<sub>140</sub>
His<sub>86</sub>

$$Fe^{+3}$$
 $Glu_{93}$ 
 $O=O$ 
 $O=O$ 
 $O=O$ 
 $O=O$ 

Figure 6. Putative binding models for C93E CDO. A. Bidentate binding of L-cysteine to C93E CDO. Bidentate binding of L-cysteine to C93E CDO would prevent dioxygen binding to the iron center. B. Monodentate binding of L-cysteine to C93E CDO. Monodentate binding of L-cysteine to C93E CDO could occur through coordination of the L-cysteine thiol or α-amino group of L-cysteine. C. Monodentate binding of L-cysteine to C93E CDO. D. Bidentate binding of 3-MPA to C93E CDO.

## **Accession Codes**

cysteine dioygenase: Uniprot entry, P21816. PDB: 6U4S (crosslinked wild-type CDO), 6U4V (non-crosslinked wild-type CDO), 6U4L (C93E CDO).

acireductone dioxygenase: Uniprot entry, Q9ZFE7. PDB: 2HJI.

### **Supporting Information**

Figure S1: SDS-PAGE of wild-type and C93E CDO.

Figure S2: Circular dichroism spectra of wild-type and C93E CDO.

**Figure S3**: Steady-state kinetic plots of wild-type and C93E CDO.

### Acknowledgements

Research reported in this publication was made possible by funds from the National Institute of Health (R01 GM127665) and National Science Foundation (CHE-1904494 and CHE-1403293) to ALL. Use of the Stanford Synchrotron Radiation Lightsource, SLAC National Accelerator Laboratory, is supported by the U.S. Department of Energy, Office of Science, Office of Basic Energy Sciences under Contract No. DE-AC02-76SF00515. The SSRL Structural Molecular Biology Program is supported by the DOE Office of Biological and Environmental Research, and by the NIH and NIGMS (including P41GM103393). Thank you to the staff at the SSRL for their generous assistance.

#### References

- 1. Sorbo, B.; Ewetz, L. (1965) The enzymatic oxidation of cysteine to cysteinesulfinate in rat liver in *Biochem Biophys Res Commun* 18, 359-363.
- 2. Ewetz, L.; Sorbo, B. (1966) Characteristics of the cysteinesulfinate-forming enzyme system in rat liver in *Biochim Biophys Acta 128*, 296-305.
- 3. Dunwell, J. M.; Khuri, S.; Gane, P. J. (2000) Microbial relatives of the seed storage proteins of higher plants: conservation of structure and diversification of function during evolution of the cupin superfamily in *Microbiol Mol Biol Rev 64*, 153-179.
- McCoy, J. G.; Bailey, L. J.; Bitto, E.; Bingman, C. A.; Aceti, D. J.; Fox, B. G.; Phillips, G. N. J. (2006) Structure and mechanism of mouse cysteine dioxygenase in *Proc Natl Acad Sci U S A 103*, 3084-3089.
- 5. Simmons, C. R.; Liu, Q.; Huang, Q.; Hao, Q.; Begley, T. P.; Karplus, P. A.; Stipanuk, M. H. (2006) Crystal structure of mammalian cysteine dioxygenase. A novel mononuclear iron center for cysteine thiol oxidation in *J Biol Chem 281*, 18723-18733.
- 6. Gane, P. J.; Dunwell, J. M.; Warwicker, J. (1998) Modeling based on the structure of vicilins predicts a histidine cluster in the active site of oxalate oxidase in *J Mol Evol 46*, 488-493.
- 7. Oka, T.; Simpson, F. J. (1971) Quercetinase, a dioxygenase containing copper in *Biochem Biophys Res Commun* 43, 1-5.
- 8. Dai, Y.; Wensink, P. C.; Abeles, R. H. (1999) One protein, two enzymes in *J Biol Chem* 274, 1193-1195.
- 9. Schaab, M. R.; Barney, B. M.; Francisco, W. A. (2006) Kinetic and spectroscopic studies on the quercetin 2,3-dioxygenase from *Bacillus subtilis* in *Biochemistry* 45, 1009-1016.
- 10. Moomaw, E. W.; Angerhofer, A.; Moussatche, P.; Ozarowski, A.; García-Rubio, I.; Richards, N. G. (2009) Metal dependence of oxalate decarboxylase activity in *Biochemistry* 48, 6116-6125.
- 11. Uberto, R.; Moomaw, E. W. (2013) Protein similarity networks reveal relationships among sequence, structure, and function within the Cupin superfamily in *PLoS One 8*, e74477.
- 12. Dunwell, J. M.; Purvis, A.; Khuri, S. (2004) Cupins: the most functionally diverse protein superfamily in *Phytochemistry* 65, 7-17.
- 13. Woo, E. J.; Dunwell, J. M.; Goodenough, P. W.; Marvier, A. C.; Pickersgill, R. W. (2000) Germin is a manganese containing homohexamer with oxalate oxidase and superoxide dismutase activities in *Nat Struct Biol* 7, 1036-1040.
- 14. Ju, T.; Goldsmith, R. B.; Chai, S. C.; Maroney, M. J.; Pochapsky, S. S.; Pochapsky, T. C. (2006) One protein, two enzymes revisited: a structural entropy switch interconverts the two isoforms of acireductone dioxygenase in *J Mol Biol 363*, 823-834.
- 15. Al-Mjeni, F.; Ju, T.; Pochapsky, T. C.; Maroney, M. J. (2002) XAS investigation of the structure and function of Ni in acireductone dioxygenase in *Biochemistry* 41, 6761-6769.
- Koehntop, K. D.; Emerson, J. P.; Que, L. (2005) The 2-His-1-carboxylate facial triad: a versatile platform for dioxygen activation by mononuclear non-heme iron(II) enzymes in J Biol Inorg Chem 10, 87-93.
- 17. Chai, S. C.; Jerkins, A. A.; Banik, J. J.; Shalev, I.; Pinkham, J. L.; Uden, P. C.; Maroney, M. J. (2005) Heterologous expression, purification, and characterization of recombinant rat cysteine dioxygenase in *J Biol Chem 280*, 9865-9869.
- 18. Simmons, C. R.; Hirschberger, L. L.; Machi, M. S.; Stipanuk, M. H. (2006) Expression, purification, and kinetic characterization of recombinant rat cysteine dioxygenase, a non-

- heme metalloenzyme necessary for regulation of cellular cysteine levels in *Protein Expr Purif* 47, 74-81.
- 19. Stipanuk, M. H.; Londono, M.; Hirschberger, L. L.; Hickey, C.; Thiel, D. J.; Wang, L. (2004) Evidence for expression of a single distinct form of mammalian cysteine dioxygenase in *Amino Acids* 26, 99-106.
- Dominy, J. E.; Hwang, J.; Guo, S.; Hirschberger, L. L.; Zhang, S.; Stipanuk, M. H. (2008) Synthesis of amino acid cofactor in cysteine dioxygenase is regulated by substrate and represents a novel post-translational regulation of activity in *J Biol Chem* 283, 12188-12201.
- 21. Njeri, C. W.; Ellis, H. R. (2014) Shifting redox states of the iron center partitions CDO between crosslink formation or cysteine oxidation in *Arch Biochem Biophys* 558, 61-69.
- 22. Ye, S.; Wu, X.; Wei, L.; Tang, D.; Sun, P.; Bartlam, M.; Rao, Z. (2007) An insight into the mechanism of human cysteine dioxygenase. Key roles of the thioether-bonded tyrosine-cysteine cofactor in *J Biol Chem* 282, 3391-3402.
- 23. Driggers, C. M.; Kean, K. M.; Hirschberger, L. L.; Cooley, R. B.; Stipanuk, M. H.; Karplus, P. A. (2016) Structure-based insights into the role of the Cys-Tyr crosslink and inhibitor recognition by mammalian cysteine dioxygenase in *J Mol Biol 428*, 3999-4012.
- 24. Li, W.; Blaesi, E. J.; Pecore, M. D.; Crowell, J. K.; Pierce, B. S. (2013) Second-sphere interactions between the C93-Y157 cross-link and the substrate-bound Fe site influence the O(2) coupling efficiency in mouse cysteine dioxygenase in *Biochemistry* 52, 9104-9119.
- 25. Arjune, S.; Schwarz, G.; Belaidi, A. A. (2015) Involvement of the Cys-Tyr cofactor on iron binding in the active site of human cysteine dioxygenase in *Amino Acids* 47, 55-63.
- 26. Davies, C. G.; Fellner, M.; Tchesnokov, E. P.; Wilbanks, S. M.; Jameson, G. N. (2014) The Cys-Tyr cross-link of cysteine dioxygenase changes the optimal pH of the reaction without a structural change in *Biochemistry 53*, 7961-7968.
- 27. Dominy, J. E. J.; Hwang, J.; Guo, S.; Hirschberger, L. L.; Zhang, S.; Stipanuk, M. H. (2008) Synthesis of amino acid cofactor in cysteine dioxygenase is regulated by substrate and represents a novel post-translational regulation of activity in *J Biol Chem* 283, 12188-12201.
- 28. Leitgeb, S.; Nidetzky, B. (2008) Structural and functional comparison of 2-His-1-carboxylate and 3-His metallocentres in non-haem iron(II)-dependent enzymes in *Biochem Soc Trans* 36, 1180-1186.
- 29. Imsand, E. M.; Njeri, C. W.; Ellis, H. R. (2012) Addition of an external electron donor to in vitro assays of cysteine dioxygenase precludes the need for exogenous iron in *Arch Biochem Biophys* 521, 10-17.
- 30. Vanoni, M. A.; Edmondson, D. E.; Zanetti, G.; Curti, B. (1992) Characterization of the flavins and the iron-sulfur centers of glutamate synthase from *Azospirillum brasilense* by absorption, circular dichroism, and electron paramagnetic resonance spectroscopies in *Biochemistry 31*, 4613-4623.
- 31. McPhillips, T. M.; McPhillips, S. E.; Chiu, H. J.; Cohen, A. E.; Deacon, A. M.; Ellis, P. J.; Garman, E.; Gonzalez, A.; Sauter, N. K.; Phizackerley, R. P.; Soltis, S. M.; Kuhn, P. (2002) Blu-Ice and the Distributed Control System: software for data acquisition and instrument control at macromolecular crystallography beamlines in *J Synchrotron Radiat 9*, 401-406.
- 32. Kabsch, W. (2010) XDS in Acta Crystallogr D Biol Crystallogr 66, 125-132.
- 33. Adams, P. D.; Grosse-Kunstleve, R. W.; Hung, L. W.; Ioerger, T. R.; McCoy, A. J.; Moriarty, N. W.; Read, R. J.; Sacchettini, J. C.; Sauter, N. K.; Terwilliger, T. C. (2002) PHENIX: building new software for automated crystallographic structure determination in *Acta Crystallogr D Biol Crystallogr 58*, 1948-1954.

- 34. Emsley, P.; Cowtan, K. (2004) Coot: model-building tools for molecular graphics in *Acta Crystallogr D Biol Crystallogr 60*, 2126-2132.
- 35. Chai, S. C.; Bruyere, J. R.; Maroney, M. J. (2006) Probes of the catalytic site of cysteine dioxygenase in *J Biol Chem 281*, 15774-15779.
- 36. Dominy, J. E.; Simmons, C. R.; Karplus, P. A.; Gehring, A. M.; Stipanuk, M. H. (2006) Identification and characterization of bacterial cysteine dioxygenases: a new route of cysteine degradation for eubacteria in *J Bacteriol* 188, 5561-5569.
- 37. Crawford, J. A.; Li, W.; Pierce, B. S. (2011) Single turnover of substrate-bound ferric cysteine dioxygenase with superoxide anion: enzymatic reactivation, product formation, and a transient intermediate in *Biochemistry* 50, 10241-10253.
- 38. Pierce, B. S.; Gardner, J. D.; Bailey, L. J.; Brunold, T. C.; Fox, B. G. (2007) Characterization of the nitrosyl adduct of substrate-bound mouse cysteine dioxygenase by electron paramagnetic resonance: electronic structure of the active site and mechanistic implications in *Biochemistry 46*, 8569-8578.
- 39. Simmons, C. R.; Krishnamoorthy, K.; Granett, S. L.; Schuller, D. J.; Dominy, J. E. J.; Begley, T. P.; Stipanuk, M. H.; Karplus, P. A. (2008) A putative Fe<sup>2+</sup>-bound persulfenate intermediate in cysteine dioxygenase in *Biochemistry* 47, 11390-11392.
- 40. Driggers, C. M.; Cooley, R. B.; Sankaran, B.; Hirschberger, L. L.; Stipanuk, M. H.; Karplus, P. A. (2013) Cysteine dioxygenase structures from pH 4 to 9: consistent cys-persulfenate formation at intermediate pH and a Cys-bound enzyme at higher pH in *J Mol Biol 425*, 3121-3136.
- 41. Dunwell, J. M.; Culham, A.; Carter, C. E.; Sosa-Aguirre, C. R.; Goodenough, P. W. (2001) Evolution of functional diversity in the cupin superfamily. *Trends Biochem Sci* 26, 740-746.
- 42. Levin, E. J.; Kondrashov, D. A.; Wesenberg, G. E.; Phillips, G. N. (2007) Ensemble refinement of protein crystal structures: validation and application in *Structure 15*, 1040-1052.
- 43. Just, V. J.; Stevenson, C. E.; Bowater, L.; Tanner, A.; Lawson, D. M.; Bornemann, S. (2004) A closed conformation of *Bacillus subtilis* oxalate decarboxylase OxdC provides evidence for the true identity of the active site in *J Biol Chem 279*, 19867-19874.
- 44. Cleasby, A.; Wonacott, A.; Skarzynski, T.; Hubbard, R. E.; Davies, G. J.; Proudfoot, A. E.; Bernard, A. R.; Payton, M. A.; Wells, T. N. (1996) The x-ray crystal structure of phosphomannose isomerase from *Candida albicans* at 1.7 angstrom resolution in *Nat Struct Biol* 3, 470-479.
- 45. Kruidenier, L.; Chung, C. W.; Cheng, Z.; Liddle, J.; Che, K.; Joberty, G.; Bantscheff, M.; Bountra, C.; Bridges, A.; Diallo, H.; Eberhard, D.; Hutchinson, S.; Jones, E.; Katso, R.; Leveridge, M.; Mander, P. K.; Mosley, J.; Ramirez-Molina, C.; Rowland, P.; Schofield, C. J.; Sheppard, R. J.; Smith, J. E.; Swales, C.; Tanner, R.; Thomas, P.; Tumber, A.; Drewes, G.; Oppermann, U.; Patel, D. J.; Lee, K.; Wilson, D. M. (2012) A selective jumonji H3K27 demethylase inhibitor modulates the proinflammatory macrophage response in *Nature 488*, 404-408.
- 46. Lombardini, J. B.; Singer, T. P.; Boyer, P. D. (1969) Cysteine oxygenase. II. Studies on the mechanism of the reaction with 18oxygen in *J Biol Chem 244*, 1172-1175.
- 47. Wang, Y.; Griffith, W. P.; Li, J.; Koto, T.; Wherritt, D. J.; Fritz, E.; Liu, A. (2018) Cofactor Biogenesis in Cysteamine Dioxygenase: C-F Bond Cleavage with Genetically Incorporated Unnatural Tyrosine in *Angew Chem Int Ed Engl* 57, 8149-8153.

- 48. Driggers, C. M.; Hartman, S. J.; Karplus, P. A. (2015) Structures of Arg- and Gln-type bacterial cysteine dioxygenase homologs in *Protein Sci* 24, 154-161.
- 49. Pierce, B. S.; Subedi, B. P.; Sardar, S.; Crowell, J. K. (2015) The "Gln-Type" thiol dioxygenase from *Azotobacter vinelandii* is a 3-mercaptopropionic acid dioxygenase in *Biochemistry* 54, 7477-7490.
- 50. Li, J, Koto, T., Davis, I. and Liu, A. (2019) Probing the Cys-Tyr Cofactor Biogenesis in Cysteine Dioxygenase by the Genetic Incorporation of Fluorotyrosine in *Biochemistry* 58, 2218-2227.
- 51. Fellner, M.; Aloi, S.; Tchesnokov, E. P.; Wilbanks, S. M.; Jameson, G. N. (2016) Substrate and pH-Dependent Kinetic Profile of 3-Mercaptopropionate Dioxygenase from *Pseudomonas aeruginosa* in *Biochemistry* 55, 1362-1371.
- 52. Yamaguchi, K.; Hosokawa, Y.; Kohashi, N.; Kori, Y.; Sakakibara, S.; Ueda, I. (1978) Rat liver cysteine dioxygenase (cysteine oxidase). Further purification, characterization, and analysis of the activation and inactivation in *J Biochem 83*, 479-491.
- 53. Li, W.; Pierce, B. S. (2015) Steady-state substrate specificity and O<sub>2</sub>-coupling efficiency of mouse cysteine dioxygenase in *Arch Biochem Biophys* 565, 49-56.
- 54. Williams, C; Hintze, B. J.; Headd, J. J., Moriarty, N. W., Chen, V. B., Jain, S.; Prisant, M. G.; Lewis, S.M., Videau, L. L.: Keedy, D. A.; Deis, L. N.; Arendall, W.B. III; Verma, V.; Snoeyink, J. S.; Adams, P. D.; Lovell, S. C.; Richardson, J. S.; Richardson, D.C. (2018) *MolProbity: More and better reference data for improved all-atom structure validation* in *Prot Sci* 27 293-315.